Characterization of Bi substitution of strontium cobalt zinc ferrites synthesized by micro-emulsion technique

G. Rasool[a], M. S. Shifa[b], H. M. N. H. K. Asghar[c], Z. A. Gilani[c,*], A. Javid[b], M. M. Alam[b], S. M. Ali[d], M. A. Shar[e], H. S. Abdo [f]
[a]*Department of physics, GC University Faisalabad*
[b]*Institute of Physics, The Islamia University of Bahawalpur*
[c]*Department of Physics, Balochistan University of Information Technology, Engineering & Management Sciences, Quetta 87300, Pakistan*
[d]*Department of Physics and Astronomy, College of Science, P.O. BOX 2455, King Saud University, Riyadh, 11451, Saudi Arabia*
[e]*Department of Mechanical & Energy Systems Engineering, Faculty of Engineering and Informatics, University of Bradford, Bradford BD7 1DP, United Kingdom*
[f]*Mechanical Engineering Department, College of Engineering, King Saud University, Riyadh 11421, Saudi Arabia*

Strontium cobalt zinc bismuth ferrites with formula are provided in this study using formula $Sr_{0.5}Co_{0.4}Zn_{0.4}Bi_xFe_{2-x}O_4$ at different variation of x= 0.0, 0.05, 0.10, 0.15 synthesized by Micro-emulsion techniques. To check the physical characteristics of this series ($Sr_{0.5}Co_{0.4}Zn_{0.4}Bi_xFe_{2-x}O_4$) of nano-ferrites using FTIR (Fourier Transformation of infrared spectroscopy), UV-visible, X-ray diffraction and scanning electron microscope. SEM and XRD analysis were used to examine the structure and morphology of manufactured nano-ferrites. The spectra of XRD demonstrated the production of a single-phase cubic spinel ferrite structure in the nanometer size range with no minor phase. When extending metal-oxygen bonds at tetrahedral and octahedral sites, FTIR analysis showed two bands centered at 592 and 410 cm^{-1}. Using ultraviolet-DRS, we determined that band-gap range for the synthesised magnetic materials was between 2.42 and 2.32 eV.

(Received October 17, 2023; Accepted December 5, 2023)

Keywords: Co-Zn, Bismuth, Nano ferrites, Micro-emulsion, XRD, SEM, UV

1. Introduction

Some of the most widely used magnetic materials are spinel ferrites, which have a chemical formula MFe_2O_4 where M denotes Manganese, Magnesium, Zinc, Nickle, and Cobalt. These materials are associated with increased performance in high-frequency devices due to their magnetic behavior, correlated nature, and structural properties[1, 2]. A few studies examined the impact of adding Bi^{3+} to CFO. The spinel structure of CFO is predicted to be unaffected by the replacement of a small quantity of Bi^{3+}. At a Bi^{3+} concentration of 0.1 or above, however, Bi^{3+} replaces Fe^{3+} in the octahedral position, resulting in improved electrical characteristics, reduced magnetic anisotropy, and reduced saturation magnetization.[3, 4]. Bismuth ferrite is recognized as a single-phase multiferroic material distinguished by its high electrical resistivity and minimal magnetic and dielectric losses [5].Because of its exceptional multiferroic characteristics at ambient temperature, bismuth ferrite (BiFeO3) with a rhombohedral distorted perovskite crystal structure has piqued the interest of researchers in recent years[6].Ferrites are magnetic and electrically active ferrimagnetic materials[7].New compounds, such as Bi^{3+} substituted ferrites, have recently been created that have outstanding electromagnetic characteristics and low dielectric loss. Multiferroics, such as Cr_2O_3 and $BiFeO_3$, are naturally occurring single-phase materials showing magnetization and electric polarization[8,

* Corresponding author: zagilani2002@yahoo.com
https://doi.org/10.15251/JOR.2023.196.695

9].Furthermore, spinel ferrites have been utilized to improve biosensors' sensitivity and stability for various applications, including clinical, food, and environmental evaluations[10].Bi-doped YIG garnets ($Y_{3-x}Bi_xFe_5O_{12}$) were recommended for usage in industrial applications such as inductors, isolators, filters, and RF devices in other investigations[11].The spinel oxide family includes cobalt ferrite ($CoFe_2O_4$). In each unit cell, there are 32 oxygen ions, along with 8 cobalt ions and iron ions, giving it a face-centered cubic structure. In the oxygen ion lattice, there are sixty four tetra-hedral, thirty two octa-hedral, and twenty four cations. In the crystal structure, half of the octahedral sites are occupied by eight Co2+ cations and eight Fe3+ cations, while the remaining eight Fe3+ ions occupy eight of the 64 tetrahedral sites. An example of an inverted spinel structure is $CoFe_2O_4$[12]. Nanoparticles are used in various disciplines, including biological applications like rug delivery[13].Because of their different properties and functions, the ironstone spinel ferrites retain their magnetic iron oxide[14]. Concerning these routines to practical treatment, the nanoparticles links numerous influence; (i) size of particles, (ii) cation dispersion in tetrahedral (A) and octahedral (B) spinel structures[15]. Among the alteration metal spinel ferrites, $CoFe_2O_4$ exists individual of the best elevation magnetization [16]. Similarly, $ZnFe_2O_4$ is auspicious measurable due to matchless categories and their penchant for Sp^3 attachment through oxygen ions, essentially to very high electrical resistivity [17]. As a result, $CoZnFe_2O_4$ retains dispersed assets aimed at numerous varieties of electromagnetic tender [18]. While the favorable properties of these spinel ferrites, damages continue to extensively disadvantage popular the ferrites materials since of their accurate consequence to the constituent proposal. The latest products to vital components are ferrites such that floppy drives, notebook computer, hard temperature. The ferrites are used to audio and visual equipment. Another uses of these ferrites to usesthat liquid of crystal TV set and auto-mobile phones etc. Application of these ferrites asthedifferent applications of ferrite is given that high frequency transformer core and computer core memoirs. Ferrites likewise show good dielectric characteristics. The moral dielectric properties nasty that container pass electromagnetic seas through them without showing electricity. That property stays not originate in warm field. Especially the crystal-like ferrites show single besides dielectrically properties. This research documents the impact of Bi^{2+} substitution on the magnetic and electrical properties of strontium cobalt zinc ferrites. The samples were prepared using Micro-emulsion techniques. We intended to inspect the part of top to our knowledge, around is no evidence nearby influence of Bi^{2+} doping on $Sr_{0.5}Co_{0.4}Zn_{0.4}Bi_xFe_{2-x}O_4$ at different variation of x= 0.0, 0.05, 0.10, 0.15 toward form a Nanoparticle. Accordingly, an illustrated investigation aimed at cation distribution, morphology analysis, considered for fundamental and visual properties. When compared to other synthesis methods such as ball milling and sol-gel vapours phase installation, this validated the clarity of the phase as well as uniformity and particle size laterally through a reduced number of flaws. To check the physical characteristics of this series ($Sr_{0.5}Co_{0.4}Zn_{0.4}Bi_xFe_{2-x}O_4$) of Nano-ferrites using FTIR, Ultraviolet visible, XRD and SEM spectroscop. Nano-ferrites were analyzed for their shape and structure using scanning electron microscopy and X-ray diffraction techniques. The XRD pattern demonstrated the formation of a single-phase cubic spinel ferrite structure with no minor phase in the nm size range. The samples were characterized using X-rays to investigate the structural alterations that occurred because of the dopant.

2. Experimental procedures

The $Sr_{0.5}Co_{0.4}Zn_{0.4}Bi_xFe_{2-x}O_4$ at different variation of x = 0.0, 0.05, 0.10, 0.15 synthesized by Micro-emulsion techniques [19]. For the preparation, the following substances were used:$Sr_{0.5}Co_{0.4}Zn_{0.4}Bi_xFe_{2-x}O_4$ nanocrystalline ferrites; Co $(NO_3)_3.6HO_2$ (99%, sigma Aldrich), $H_{12}Cl_2O_6Sr$ (98%, sigmaAldrich), Zn (NO3)2.6H2O (98%, sigma Aldrich), Bismuth, Fe $(NO_3)_3.9H_2O$ (98%, sigma Aldrich), Cetyl-trimethl-ammonium bromide, aqueous sodium-hydroxide (NaOH), BDH, deionized water. The appropriate quantities of metal salt solutions (0.15M) were mixed and stirred on a magnetic hot plate at 50-60°C. The surfactant was a CTAB aqueous solution (100ml, 0.45M). NaOH was used to adjust the pH and maintain it between 11 and 12 for all of the components. For another 4-5 hour, we stirred the reaction mixture. Deionized water was used to

wash the precipitates until the pH was decreased to 7. A 100℃ oven was used to evaporate the water, and with a Vulcan A-550 muffle furnace with temperature control was used to anneal the metal for 7 hours at a temperature of 700℃. The materials were characterised using a number of techniques after being ground into powder. Powder XRD analysis was conducted using a Philips 'X' Pert PRO 3040/60 diffractometer with CuK α as the radiation source to verify the synthesis materials purity. FTIR spectrum, where the FT-IR spectra were seen using a Perkin Elmer spectrometer. UV-visible at room temperature, spectroscopy was employed to investigate the same. Details of the instruments may be viewed[20, 21]. Scanning electron microscopy SM- 6590 LV Japan was used to examine particle morphology.

3. Results and discussion

3.1. The structural analysis

The XRD spectra of Bismuth substituted SrCoZn ferrites are shown in Figure 1. The following peaks were detected and successfully identified using the formulas (111), (200), (220), (311), (222), (400), (422), (511), (440), (620), and (533)(2)were used for calculating the lattice parameter is given above [22], which planes characterise the single-phase cubic spinel structure [23, 24] solubility of cations in their respective lattice locations is shown. According to this technique to study those defects, inter plane distance, material quality, crystal structure, crystal size and lattice parameters. The crystalline resources retain representative patterns which remain respectable source of enquiry in substantial sciences to use X-rays diffracted, other using Bragg's Law. Scherer's formula was used to find the general formula for calculating a= lattice constant, D= crystallite size, d=inter-plane distance, $d_{x\text{-}ray}$ = X-ray density (ρx) , and the size of the crystallite of all samples[25, 26];

$$D = \frac{K\lambda}{\beta_{hkl} COS\theta} \tag{1}$$

$$a = \frac{\lambda}{2Sin\theta}\sqrt{h^2 + k^2 + l^2} \tag{2}$$

Other formula to find out of lattice constant.

$$a = d\sqrt{h^2 + k^2 + l^2} \tag{3}$$

$$d = \frac{\lambda}{2Sin\theta} \tag{4}$$

$$d_{x-ray} = \frac{ZM}{N_A V} \tag{5}$$

where "λ" it is denoted by wavelength of X-ray, "h", "k", "l" represents the miller indices of certain plane, "k" designates the shape factor, and "V" denotes cell volume. Where "β_{hkl}" symbolizes the FWHM of the specific plane., "$N_A = 6.02 \times 10^{23}$ g/mol" denotes the Avogadro's numbers, "M" to characterizes the molecular mass and "Z" signifies the fragments per unit cell of spinel organization. The crystalline size remains establish to drops since 41.08 near 30.79 nm equally the meditation of Bi growths in the range of(x = 0.0 to 0.15), revealed in figure 1. The lattice constant was reduced from 8.378 to 8.372 after Bi^{2+} substitution, and cell volume was similarly reduced from 588.05 to 58.79. Completely tested ingredient densities remained lower than X-ray densities. This denotes the presence of nanocrystalline apertures that were generated in addition to those that were established throughout the section provision. The porosity values were determined to be in the 0.48 to 0.54 range.

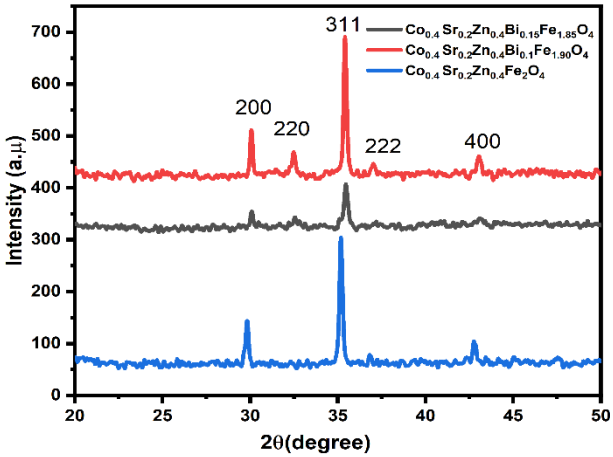

Fig 1. XRD pattern of synthesized samples $Sr_{0.5}Co_{0.4}Zn_{0.4}Bi_xFe_{2-x}O_4$.

Table 1. Porosity and crystallite size, as well as lattice constant, cell volume, bulk density, and X-ray density.

Bi concentration (x)	0.00	0.01	0.10	0.15
Lattice constant (Å)	8.378	8.376	8.375	8.372
CellVolume (V_{cell}) $(Å)^3$	588.05	587.63	587.42	586.79
Bulk Density ρx (g/cm^3)	2.52	2.33	2.27	2.21
X-ray Density ρ_b (g/cm^3)	4.83	4.81	4.79	4.78
Porosity (%)	0.48	0.52	0.53	0.54
Crystallite size (nm)	41.08	38.34	33.69	30.79

3.2. FTIR (Fourier Transform infrared spectrum analysis)

Infrared spectroscopy may be done in a variety of ways, but FTIR spectra is particularly useful. To determine where ions are located in a crystal, FTIR analysis is important. Chemical changes in and cation distribution at sites were identified using FTIR spectra[27].The Fourier Transform infrared spectroscopy (FTIR) perceived bands confirm that structure of strontium cobalt zinc bismuth ferrite. Fig. 2 shows the respective FT-IR spectra of $Sr_{0.5}Co_{0.4}Zn_{0.4}Bi_xFe_{2-x}O_4$ at different variation of x= 0.0, 0.05, 0.10, 0.15[28]. The FTIR spectra of Sr based nanoparticles are displayed in Figure 5, and they exhibit two distinct bands in 4000 to 500 cm^{-1} region [29]. which is a spinel structure's distinctive band. These graphs consist of different absorption bands range 4000-500 cm^{-1}. The absorption band value 403-592 cm^{-1} to show that metal oxygen. The weak bands about at 1379 and 1365 cm^{-1} to present the nitrate group. Absorption band at 2918 and 2911 cm^{-1} are given to stretching C-H group. The peaks round about 3424 and 1632 represent the hydroxyl group. Because of the replacement of lighter Bi ions for Fe ions, the tetrahedral extending constancy band slightly alters near to the high frequency province to promote Bi^{2+} substitution devotion, as seen in figure 5. The absorption bands acquired in the extant revision is reliable to detect that the figure to increase in Bi fixing attention, the tetrahedral extending regularity band (ν1) because of the replacement of lighter Bi ions for Fe ions towards the advanced frequency province, there are small alterations[28].

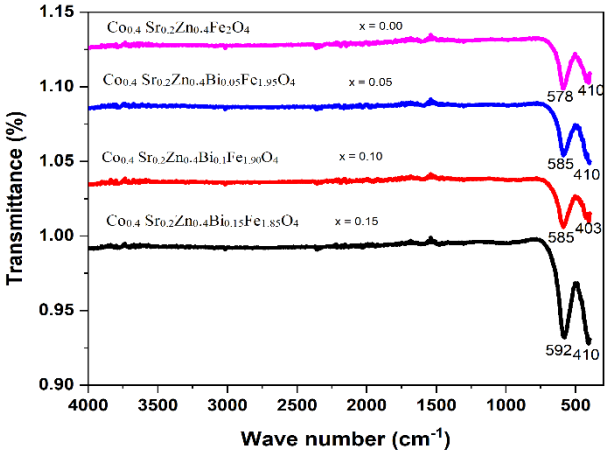

Fig. 2. Fourier Transform infrared,(FTIR) graph of $Co_{0.4}Sr_{0.2}Zn_{0.4}Bi_xFe_{2-x}O_4$.

3.3. Ultraviolet–visible spectroscopy (UV-Vis):

The visual property is the equipped magnetic nanomaterials was scanned concluded the Ultraviolet–visible analysis. The band gap energy of these sample $Co_{0.4}$ $Sr_{0.2}Zn_{0.4}Fe_2O_4$(1.33 eV), $Co_{0.4}$ $Sr_{0.2}Zn_{0.4}Bi_{0.05}Fe_{1.95}O_4$ (1.44 eV), $Co_{0.4}$ $Sr_{0.2}Zn_{0.4}Bi_{0.1}Fe_{1.90}O_4$ (1.46 eV) and $Co_{0.4}$ $Sr_{0.2}Zn_{0.4}Bi_{0.15}Fe_{1.85}O_4$ (1.30 eV) premeditated consuming Tauc calculation. The band gap of these sample to calculate that from the E_g amounts by K-M model [30] and F(R) is predictable since following relation.

$$F(R) = (1 - R)^2/2R \tag{6}$$

So, "R" is reflectance and "F(R)" is the Kubelka-Munk function. Graph is connived concerning $[F(R)h\upsilon]^2$ & $h\upsilon$, interrupt value to energy band gap (E_g) that is revealed in figures 6-9.

The predictable band gap of $Co_{0.4}$ $Sr_{0.2}Zn_{0.4}Bi_xFe_{2-x}O_4$ ($x = 0.0, 0.05, 0.10, 0.15$ & 0.20) falls from 1.46 eV (pure $Co_{0.4}$ $Sr_{0.2}Zn_{0.4}Fe_2O_4$) to 1.30eV (Bi doping), as seen in Fig 3-6, which could be identified to the subsequent sub-band-gap energy phases induced by the sparse inner and border cracks in the agglomerated nano-materials[31].

The band gap effect remains influenced through several factors such that lattice strain, structural parameter, presence of impurities, crystallite size and carrier concentrations[32]. With increasing Co concentration, the structural parameter (Lattice constant) decreases, resulting in a decrease in band gap in the current research.In the visible area, the bismuth ion also improves Faraday rotation. Magneto-optic (MO) performance is enhanced by cerium ion, and propagation loss is decreased[33, 34].For the reduction of 4-nitrophenol, the catalytic activity of cobalt ferrite and bismuth substituted cobalt ferrite nanoparticles is investigated (4-NP). In the absence of a catalyst (WC), NaBH4 may reduce 4-nitrophenol to 4-aminophenol in the exitance of cobalt ferrite and bismuth substituted cobalt ferrite. After sodium borohydride was added to 4 NPs, the UV-visible spectrum showed a prominent absorbance peak at 317 nm and 400 nm. The color changed from light yellow to bright yellow when the freshly created $NaBH_4$ solution was introduced, showing that the 4-nitrophenolate ion had formed. The reaction (decolorization) began very soon after the catalyst was added. Conversion of 4-NP to 4-AP caused the absorption peak in UV-visible spectrum to move from 400 nm to 300 nm[35].

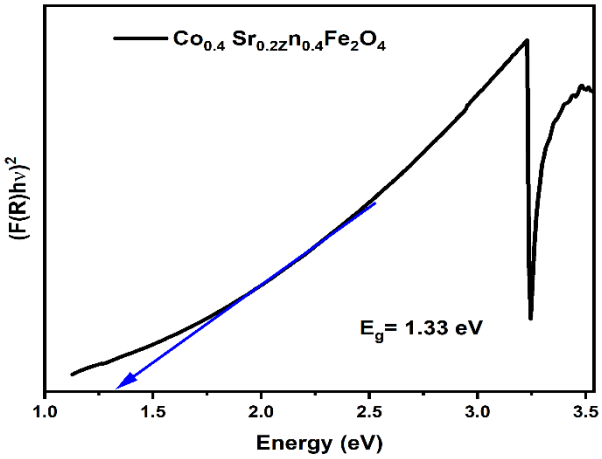

Fig. 3. Ultraviolet-Visible absorption spectra Tauc's curve of $Co_{0.4}Sr_{0.2}Zn_{0.4}Fe_2O_4$ at x = 0.00.

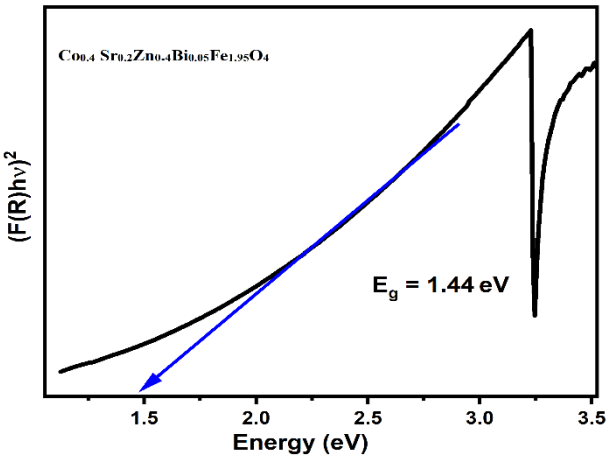

Fig. 4. Ultraviolet-Visible absorption spectra Tauc's curve of $Co_{0.4}Sr_{0.2}Zn_{0.4}Bi_{0.05}Fe_{1.95}O_4$ at x = 0.05.

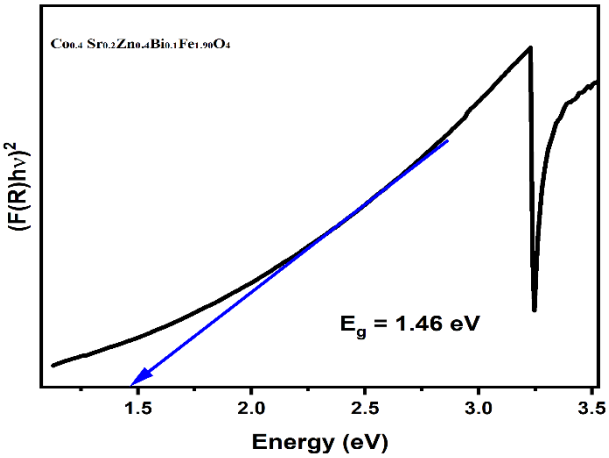

Fig. 5. UV-visible absorption spectra Tauc's curve of $Co_{0.4}Sr_{0.2}Zn_{0.4}Bi_{0.1}Fe_{1.90}O_4$ at x = 0.10.

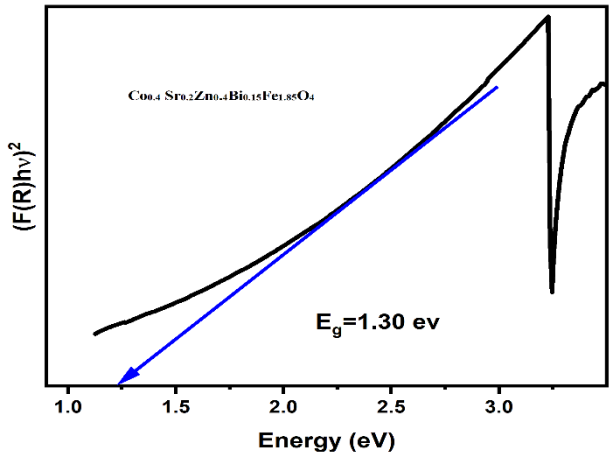

Fig. 6. UV-visible absorption spectra Tauc's curve of $Co_{0.4}Sr_{0.2}Zn_{0.4}Bi_{0.15}Fe_{1.85}O_4$ at x = 0.15.

3.4. Scanning electron microscope

SEM was employed to examine the surface morphology of the manufactured ferrite nanoparticles (NPs) to confirm their authenticity [36].The SEM investigation of usual $Sr_{0.5}Co_{0.4}Zn_{0.4}Bi_xFe_{2-x}O_4$ at different variation of x= 0.0, 0.05, 0.10, 0.15 existed done by sort field emission gun Scanning electron microscopy with model-JSM-7600F (FEG-SEM). The SEM pictures check the nanocrystalline grain development, and Fig. 7-10 displayed that a collection of crystallites ensued at a certain size during the sample provision. The particle size was firm by line intercept scheme[37], probable exhausting relation.

$$D = 1.5\, L/M \times N \tag{7}$$

where L is the overall length of the check line, M is the amplification, and N is the total number of the sample. A normal grain size (D) of $Sr_{0.5}Co_{0.4}Zn_{0.4}Bi_xFe_{2-x}O_4$ samples was of the instruction of 41.08 nm. It is manifest since SEM pictures show that the grains of Sr0.5Co0.4Zn0.4BixFe2-xO4 are nanoscale through intense holes. This is extra rewards near the gas detecting submissions as reduced grains have greater definite outward extent [38]. The voids and pores in $Sr_{0.5}Co_{0.4}Zn_{0.4}Bi_xFe_{2-x}O_4$ samples could be attributed to the release of gases during the micro-emulsion method. Reducing values of crystallite size (41.08–30.79 nm). The grain size spreading of $Sr_{0.5}Co_{0.4}Zn_{0.4}Bi_xFe_{2-x}O_4$ particles is uneven and detected in the nanometer range. The attached countryside of a few grains was observed in SEM images. The grain stem and grain frontier sorts have remained studied. Construction of the substance can be either crystalline or amorphous, with elements erratic from close to powerfully absorbent particle supplies; this disturbs the turn connection, which stays corrupt the magnetic performance [39]. The oxidation degree of 3d metals can be changed through oxygen nonstoichiometric[40].

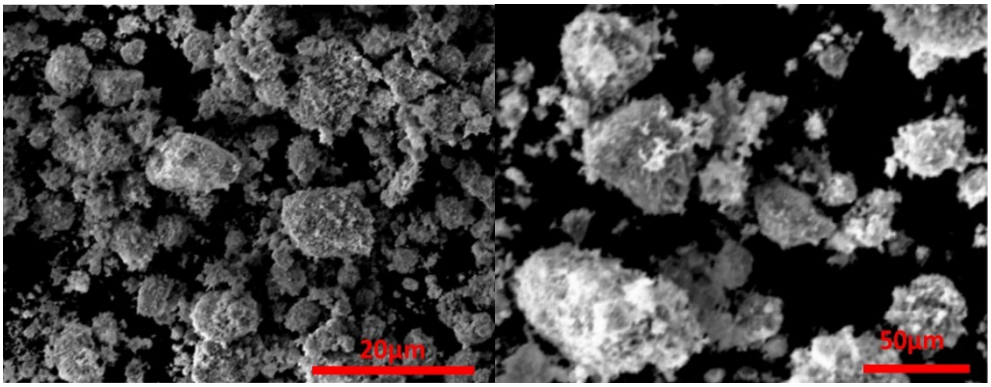

Fig. 7. SEM investigation of synthesized $Co_{0.4}$ $Sr_{0.2}Zn_{0.4}Fe_2O_4$.

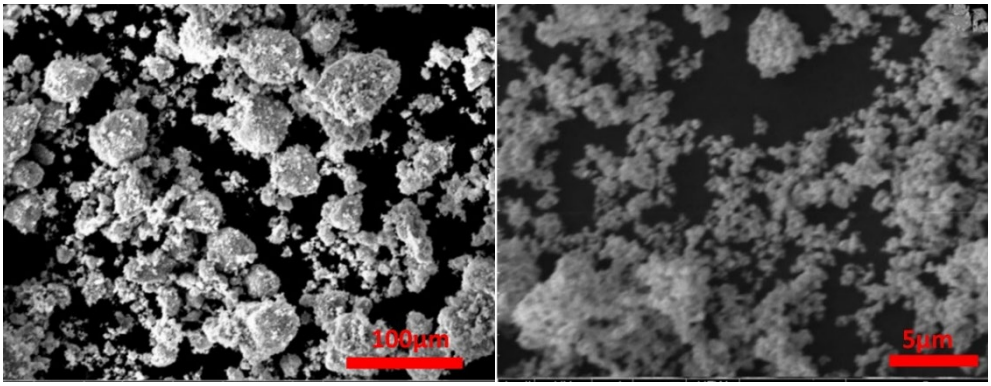

Fig. 8. SEM investigation of synthesized $Co_{0.4}\ Sr_{0.2}Zn_{0.4}Bi_{0.05}Fe_{1.95}O_4$.

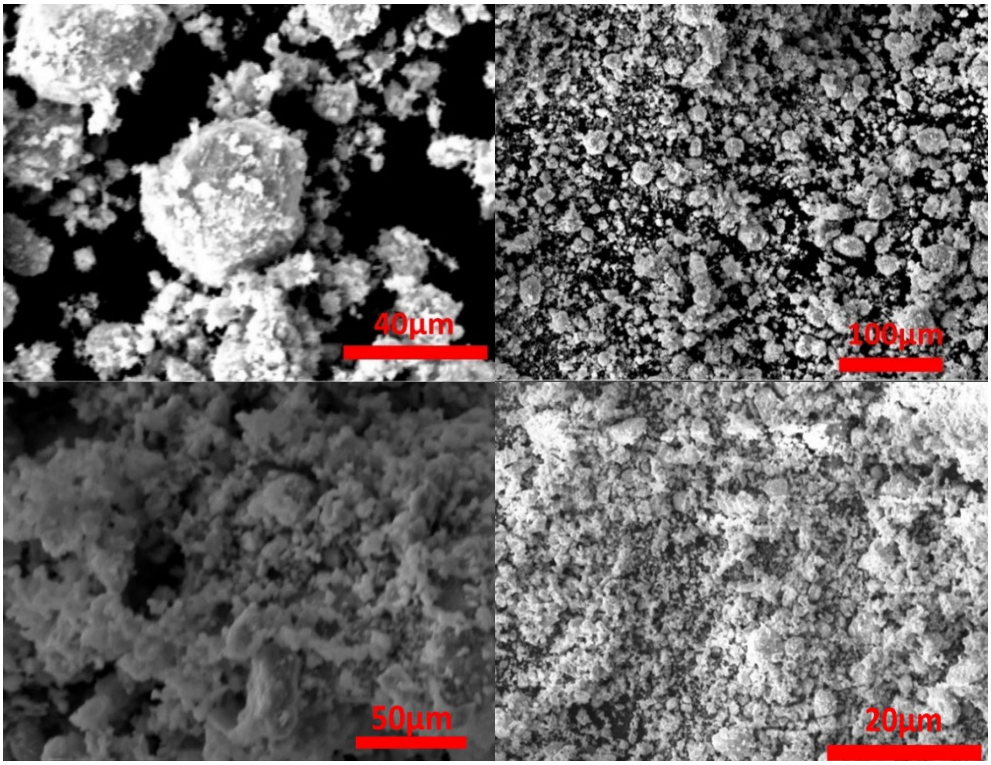

Fig. 9. SEM investigation of synthesized $Co_{0.4}\ Sr_{0.2}Zn_{0.4}Bi_{0.1}Fe_{1.90}O_4$.

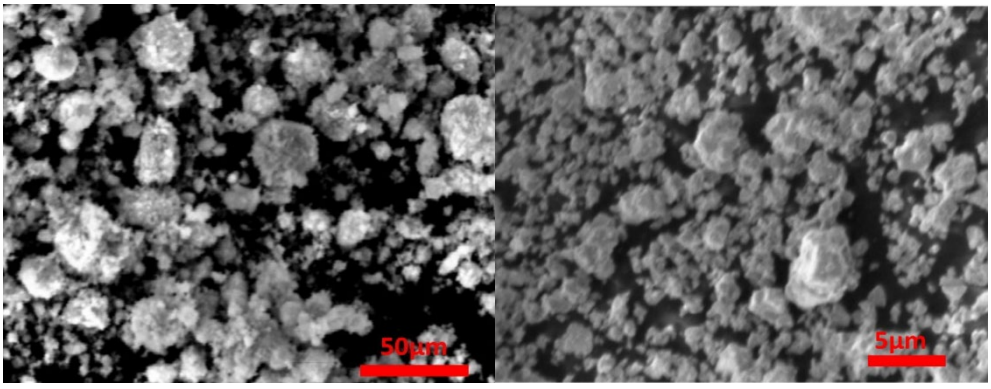

Fig. 10. SEM investigation of synthesized $Co_{0.4}\ Sr_{0.2}Zn_{0.4}Bi_{0.15}Fe_{1.85}O_4$.

4. Conclusions

Strontium cobalt zinc bismuth ferrites were synthesized through a micro-emulsion technique. The result of Bi substitution, Strsynthesized cobalt Zinc nano- crystalline determine, X-ray diffraction (XRD) checks, Single-phase crystalline structure. Crystals ranging in size from 30.79 nm to 41.08 nm were produced during the synthesis process. The crystallite size in higher-density tape medium is small enough to provide a satisfactory sign-to-noise quotient. The spectrum's Fourier transform infrared (FTIR) spectra indicate two primary absorption bands close to validating the spinel structure. When measured using ultraviolet-DRS, the band gap value of the magnetic material nanoparticles that were synthesised had a range between 2.42 and 2.32.

Acknowledgements

The authors would like to acknowledge the Researcher's Supporting Project Number (RSPD2023R1098) King Saud University, Riyadh, Saudi Arabia, for their support in this work.

References

[1] Li, F., et al., Chemistry of materials, 2004. 16(8): p. 1597-1602; https://doi.org/10.1021/cm035248c

[2] Sugimoto, M., Journal of the American Ceramic Society, 1999. 82(2): p. 269-280; https://doi.org/10.1111/j.1551-2916.1999.tb20058.x

[3] Kumar, N.S., K.V. Kumar, World Journal of Nano Science and Engineering, 2015. 5(04): p. 140; https://doi.org/10.4236/wjnse.2015.54016

[4] Gore, S.K., et al., Dalton transactions, 2015. 44(14): p. 6384-6390; https://doi.org/10.1039/C5DT00156K

[5] Eerenstein, W., N. Mathur, J.F. Scott, Nature, 2006. 442(7104): p. 759-765; https://doi.org/10.1038/nature05023

[6] Ederer, C., N.A. Spaldin, Physical Review B, 2005. 71(6): p. 060401; https://doi.org/10.1103/PhysRevB.71.060401

[7] Lakshmi, V., et al. IOP Conference Series: Materials Science and Engineering. 2019. IOP Publishing; https://doi.org/10.1088/1757-899X/577/1/012068

[8] Junaid, M., et al., Journal of Molecular Structure, 2020. 1221: p. 128859; https://doi.org/10.1016/j.molstruc.2020.128859

[9] Singh, N., A. Agarwal, S. Sanghi, Current applied physics, 2011. 11(3): p. 783-789; https://doi.org/10.1016/j.cap.2010.11.073

[10] Rocha-Santos, T.A., TrAC Trends in Analytical Chemistry, 2014. 62: p. 28-36; https://doi.org/10.1016/j.trac.2014.06.016

[11] Pardavi-Horvath, M., Journal of Magnetism and Magnetic Materials, 2000. 215: p. 171-183; https://doi.org/10.1016/S0304-8853(00)00106-2

[12] Giannakopoulou, T., et al., Journal of Magnetism and Magnetic Materials, 2002. 246(3): p. 360-365; https://doi.org/10.1016/S0304-8853(02)00106-3

[13] Veiseh, O., J.W. Gunn, M. Zhang, Advanced drug delivery reviews, 2010. 62(3): p. 284-304; https://doi.org/10.1016/j.addr.2009.11.002

[14] Barrera, G., et al., Journal of Magnetism and Magnetic Materials, 2018. 456: p. 372-380; https://doi.org/10.1016/j.jmmm.2018.02.072

[15] Tholkappiyan, R., K. Vishista, Materials Science in Semiconductor Processing, 2015. 40: p. 631-642; https://doi.org/10.1016/j.mssp.2015.06.076

[16] Vadivel, M., et al., Journal of magnetism and magnetic materials, 2014. 362: p. 122-129; https://doi.org/10.1016/j.jmmm.2014.03.016

[17] Shoba, M., S. Kaleemulla, Journal of Physics and Chemistry of Solids, 2017. 111: p. 447-457; https://doi.org/10.1016/j.jpcs.2017.08.028
[18] Huang, X., et al., Journal of Magnetism and Magnetic Materials, 2016. 405: p. 36-41; https://doi.org/10.1016/j.jmmm.2015.12.051
[19] Bayoumy, W., Journal of Molecular Structure, 2014. 1056: p. 285-291; https://doi.org/10.1016/j.molstruc.2013.10.056
[20] Thakur, P., et al., Materials Research Express, 2016. 3(7): p. 075001; https://doi.org/10.1088/2053-1591/3/7/075001
[21] Thakur, P., et al., Journal of Magnetism and Magnetic Materials, 2017. 432: p. 208-217; https://doi.org/10.1016/j.jmmm.2017.01.081
[22] Cullity, B.D., Elements of X-ray Diffraction. 1956: Addison-Wesley Publishing.
[23] Khan, M.A., et al., Ceramics International, 2011. 37(7): p. 2519-2526; https://doi.org/10.1016/j.ceramint.2011.03.063
[24] Asghar, M., K. Mahmood, M. Hasan, 2012. Trans Tech Publ.; https://doi.org/10.4028/www.scientific.net/KEM.510-511.132
[25] Sathyamoorthy, R., et al., Journal of Alloys and Compounds, 2010. 493(1-2): p. 240-245; https://doi.org/10.1016/j.jallcom.2009.12.063
[26] Rama Krishna, K., K. Vijaya Kumar, C. Ravindernathgupta, Ravinder Dachepalli, Ad v Mater Phys Chem, 2012. 2: p. 149-54; https://doi.org/10.4236/ampc.2012.23022
[27] Slimani, Y., et al., Ceramics International, 2018. 44(12): p. 14242-14250; https://doi.org/10.1016/j.ceramint.2018.05.028
[28] Dabagh, S., et al., Bulletin of Materials Science, 2016. 39(4): p. 1029-1037; https://doi.org/10.1007/s12034-016-1233-8
[29] Bayramoğlu, G., M.Y. Arica, Chemical Engineering Journal, 2008. 139(1): p. 20-28; https://doi.org/10.1016/j.cej.2007.07.068
[30] Manikandan, A., et al., Ceramics International, 2013. 39(5): p. 5909-5917; https://doi.org/10.1016/j.ceramint.2013.01.012
[31] Kislov, N., et al., Materials Science and Engineering: B, 2008. 153(1-3): p. 70-77; https://doi.org/10.1016/j.mseb.2008.10.032
[32] Kale, R., C. Lokhande, Applied Surface Science, 2004. 223(4): p. 343-351; https://doi.org/10.1016/j.apsusc.2003.09.022
[33] Ibrahim, N., C. Edwards, S. Palmer, Journal of magnetism and magnetic materials, 2000. 220(2-3): p. 183-194; https://doi.org/10.1016/S0304-8853(00)00331-0
[34] Shintaku, T., A. Tate, S. Mino, Applied physics letters, 1997. 71(12): p. 1640-1642; https://doi.org/10.1063/1.120003
[35] Du, X., et al., Applied Surface Science, 2012. 258(7): p. 2717-2723; https://doi.org/10.1016/j.apsusc.2011.10.122
[36] El-Batal, A.I., et al., Journal of Photochemistry and Photobiology B: Biology, 2017. 173: p. 120-139; https://doi.org/10.1016/j.jphotobiol.2017.05.030
[37] Aghav, P., et al., Physica B: Condensed Matter, 2011. 406(23): p. 4350-4354; https://doi.org/10.1016/j.physb.2011.08.066
[38] Singh, S., et al., Materials Research Bulletin, 2012. 47(11): p. 3538-3547; https://doi.org/10.1016/j.materresbull.2012.06.064
[39] Peddis, D., et al., Chemistry-A European Journal, 2009. 15(32): p. 7822-7829; https://doi.org/10.1002/chem.200802513
[40] Trukhanov, S., et al., Journal of Low Temperature Physics, 2007. 149(3): p. 185-199; https://doi.org/10.1007/s10909-007-9507-6